JOURNAL OF AEROSPACE SOCIETY MALAYSIA

ARTICLE

VISUALIZATION OF WATER INGRESS IN ALUMINIUM HONEYCOMB SANDWICH PANEL THROUGH MODE ISOLATION OF LAMB WAVEFIELD

Muhamad Azim Azhad Shahrim [1], Shi Yn Lee [1], Jung-Ryul Lee [2], Mohammad Yazdi Harmin [1,*] and Chen Ciang Chia [2,]**

1. Department of Aerospace Engineering, Universiti Putra Malaysia, Serdang, Selangor, Malaysia.
2. Department of Aerospace Engineering, KAIST, Daejeon 34141, Republic of Korea

Correspondence: *myazdi@upm.edu.my, **chiacc@kaist.ac.kr

Abstract: Water ingress into the honeycomb cells of aerospace structures can compromise the aircraft's safety and performance. Due to this reason, detecting it as soon as possible is critical. Even though the effectiveness of guided ultrasonic wavefield propagation imaging (G-UPI) in detecting various types of damage with high resolution has already been well-demonstrated, its capability in detecting water ingress in honeycomb cells has not been investigated. In view of this, the aim of this study is to investigate the feasibility of using G-UPI to detect and visualize water ingress in the honeycomb cells by inspecting an aluminum honeycomb sandwich panel with simulated water ingress in six individual cells. Based on the results, it has been shown that isolating the A0 mode of the waves can significantly improve the visibility of the water-filled cells. Moreover, the quantitative comparison of three different visualization methods, i.e., ultrasonic energy mapping (UEM), dominant frequency amplitude mapping (DFAM), and spectral energy mapping (SEM), has revealed that SEM is the best visualization method due to its 7.2 and 1.5 times higher contrast compared to UEM and DFAM, respectively. All in all, G-UPI has been shown to be able to effectively detect water ingress. However, careful selection of a suitable wave mode and image generation algorithm is required to achieve optimal results.

Keywords: non-destructive testing; ultrasonic wave propagation; image processing; mode isolation; Lamb waves

1. Introduction

Water ingress into honeycomb cells in aerospace structures can lead to several issues. Firstly, it can cause corrosion and degradation of the structural material, leading to reduced strength and stiffness [1], [2]. Secondly, it can cause disbonding of the skin-core as well as delamination of skin, which can result in reduction or loss of load-bearing capacity [2]-[3]. Furthermore, it can cause signal blockage of radar transmission [4], which prevents external communication to the control unit. Last but not least, water accumulation in the cells can cause an increase in weight, reducing the aircraft's fuel efficiency and also possibly affecting its flight performance. All these issues are critical to the aircraft's safe operation and therefore, it is essential to detect and prevent water ingress in honeycomb cells [2][5]. Since water ingress can have severe consequences for safety and performance of aerospace structures, it is crucial to detect it in a non-destructive manner as early as possible. However, water ingress in honeycomb cells is known as a type of complex damage. It requires a very specific non-destructive testing procedure for a higher detection probability. The probability of success in detecting water ingress in a honeycomb cell depends on several factors, including the size and location of the damage, and the method applied for detection

[4]. If any water ingress is missed during the periodic inspection using common methods, then detecting the symptoms of water ingress such as moisture spots, material discoloration or microbial growth must be conducted during visual inspection. This process is time-consuming and requires laborious work to inspect the large aircraft surface. Hence, there is a need for a better inspection technique.

To date, guided ultrasonic wavefield propagation imaging (G-UPI) has shown tremendous benefits as it manages to detect a wide range of damage types with a high probability of success [6]-[7]. G-UPI offers several advantages over the traditional ultrasonic approaches such as its ability to detect damage with high-resolution imaging that leads to comparatively higher detection probability before the damage can cause significant harm. Additionally, G-UPI provides a non-destructive way of inspecting structural integrity of materials, making it an ideal choice for monitoring the critical aerospace components' health. Furthermore, G-UPI provides the capability to cover a large inspection area in a single scan, which is particularly useful for inspecting large and complex structures. High expectations have been placed on G-UPI to produce positive results in detecting water ingress due to its demonstrated ability to detect other types of damage. If G-UPI is proven capable of detecting water damage, this method will provide further evidence to support further research and development of the technique. A recent review article has pointed out that detection of water ingress in sandwiched composites has not been investigated yet using G-UPI [8]. With this knowledge, the primary objective of this study is to investigate the feasibility of using G-UPI technique for detecting water ingress in honeycomb cores. To improve the signal-to-noise ratio, a mode isolation technique that is demonstrated to successfully detect hidden corrosion [9], cracks [10], dents [11] and delamination [12] is adopted. Another objective of this study is to assess the capabilities of various image generation algorithms, i.e., ultrasonic energy mapping (UEM), dominant frequency amplitude mapping (DFAM) and spectral energy mapping (SEM), in displaying subtle water ingress with a good contrast.

2. Methodology

For the experiment, the specimen is purchased from a composites manufacturer and consisted of two pieces of flat aluminum plates and an aluminum honeycomb core, which are bonded together using epoxy glue. The thickness of the front and back plates are 1 mm and 0.5 mm thick, respectively. In the meantime, the honeycomb core has cell size of 10.4 mm and height of 15 mm. Six holes are drilled at the back side of the as-manufactured specimen using a 3 mm drill bit in a cautious manner in order to prevent any dents or over-drilling. The cell core is then fully filled with water using a syringe and covered with cellophane tape to prevent any spillage, as shown in Figure 1(a). The relative positions of the water-filled cells are shown in Figure 1(b). Only one specimen is fabricated and used for this work. Multiple water-filled cells at different positions are created to study the variation of wave interaction with the damages. The origin is located at the bottom-left corner of the scan area. Table 1 provides the locations of all water-filled cells. For easier reference, the damage will be named with 'C#' whereby 'C' represents the cell and '#' represents its cell number. The analysis for a specific cell takes the spatio-temporal data before and after it is water-filled for side-by-side comparison.

Table 1: Location of water-filled cells.

Cell No.	x-y coordinate location (mm)
1	(62.5, 40)
2	(125, 40)
3	(187.5, 40)
4	(62.5, 210)
5	(125, 210)
6	(187.5, 210)

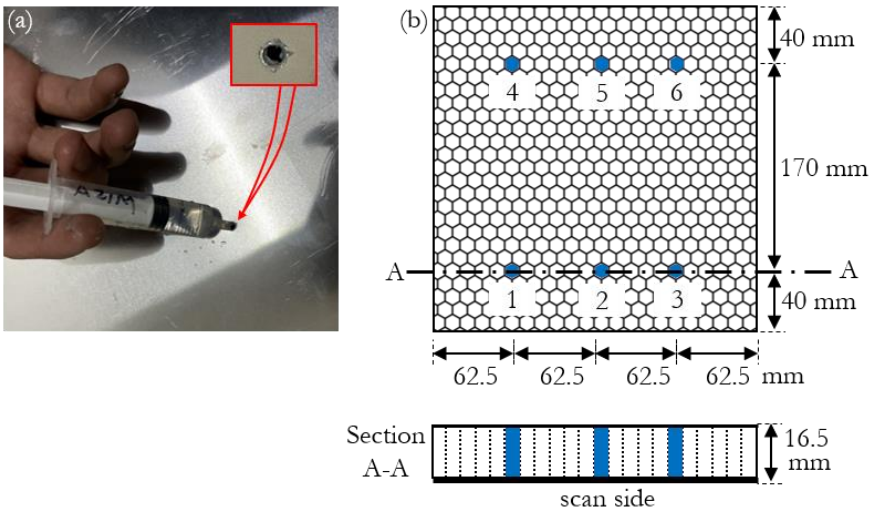

Figure 1: Infliction of damage. (a) Injection of water into a honeycomb cell through a drilled hole. (b) Relative positions of the water-filled cells. Shape and size of the internal honeycomb cells are for illustration purposes only and may differ from actual specimen.

The non-destructive inspection of the specimen is carried out using G-UPI system. Figure 2 shows the G-UPI system, which utilizes a two-dimensional (2D) laser scanning grid to generate the ultrasound and a fixed-position sensor for the measurement. The ultrasound is produced through rapid, localized thermoelastic expansion at each inspection grid point [13]. The ultrasound waves, known as the Lamb waves [14]-[15], propagated from their respective grid points, guided by the specimen boundaries, and dispersed into a mixed multimodal wave. The laser scanning is performed using a galvanometric optical scanner at a standoff distance of 1.29 m, with a pulse repetition frequency of 50 Hz. Guided waves are generated for an area of 250 by 250 mm with a uniform grid of 0.5 mm pitch in both the x (horizontal) and y (vertical) axis, resulting in a total of 250,000 grid points. Ultrasound signals are measured using a broadband, omnidirectional piezoelectric sensor that has been placed at a fixed position 125 mm above the center of the inspection area's top edge. The signals are then recorded using an oscilloscope with 500 sampling points and sampling frequency of 1.5 MHz. It should be noted that these settings of the parametric values are based on discussions in Ref. [8]. Finally, three-dimensional (3D) spatio-temporal data, v [x, y, t] is acquired from each scan.

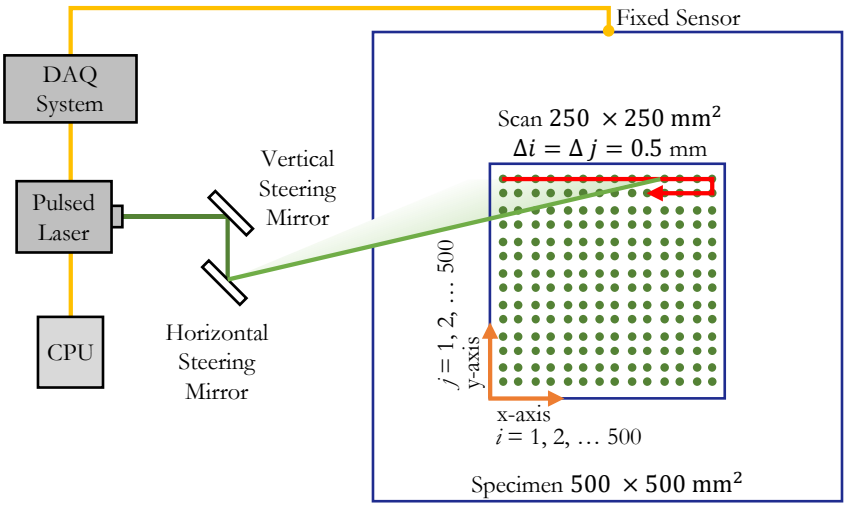

Figure 2: Schematic of the G-UPI system, specimen dimensions, inspection parameters.

As indicated earlier, the specimen used in this study has dimensions of 500 mm by 500 mm, and inspection area of 250 mm by 250 mm has been chosen at the center to reduce the effects of boundary reflections. Two repetitive scans are conducted for the specimen under eight different conditions. The repetitive scans are averaged in order to reduce noise. These eight conditions include pristine state, six holes without water, one water-filled cell, two water-filled cells and so on until all six cells are filled with water. This procedure is carried out to take a clear look at the wave behavior before and after the cells are filled with water. The captured signals are then processed using a mode-filtering algorithm to extract information about the guided ultrasonic waves, as shown in Figure 3. The processed data is later applied to generate an image to visualize internal features of the specimen, which can be interpreted to detect any damage or anomalies in the material.

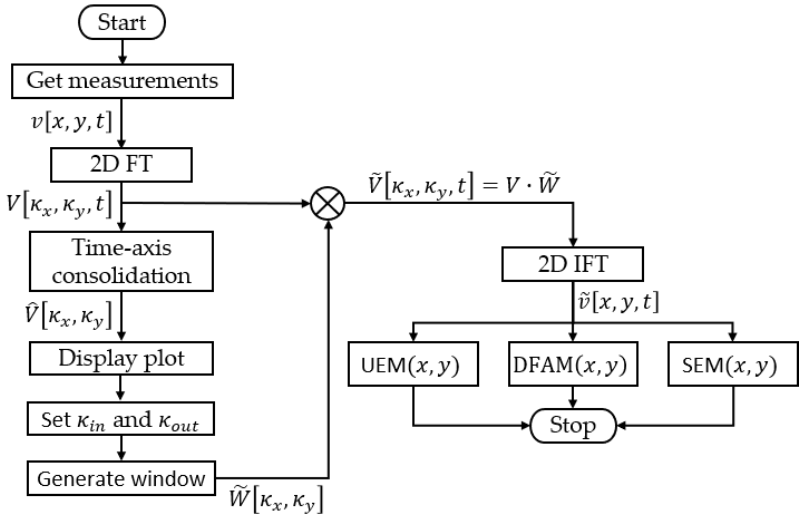

Figure 3: Flowchart of the overall result processing steps.

For mode filtering, the 3D spatio-temporal data obtained from each inspection has to undergo 2D Fourier transform (FT) in the spatial axes to convert the data into 3D wavenumber-temporal domain. A 2D FT is adopted instead of the more commonly used 3D FT [11][16] because it is found that mode filtering at similar accuracy could be obtained more efficiently using the 2D FT. After the conversion, a circular filter is generated through the function in Equation 1, where $\widetilde{W}$ represents the filter window, which is indexed by the wavenumber κ_x and κ_y along respective x or y axis, while κ_{in} and κ_{out} represent the inner and outer wavenumber values to define the circular filter, respectively, and $\kappa = \sqrt{\kappa_x{}^2 + \kappa_y{}^2}$.

$$\widetilde{W}[\kappa_x,\kappa_y] = \begin{cases} 1, & \kappa_{in} < \kappa < \kappa_{out} \\ 0, & \text{otherwise} \end{cases} \quad (1)$$

There are several choices for the filtering, either using S0 mode, A0 mode or even anomalous mode at own discretion. The selection can be made based on the plot of the consolidated wavenumber-time domain data as shown on the left side of Figure 4. In this plot, the consolidated energy of the S0 and A0 modes can be identified over the black background as two concentric rings, i.e., S0 as the inner ring while A0 as the outer ring. Depending on the desired mode, the values of filter parameters κ_{in} and κ_{out} can be determined through visual inspection of the consolidated wavenumber-time domain data. As an illustration to aid understanding, a filter window suitable for the isolation of A0 mode is generated using Equation 1 and shown in the middle plot of Figure 4. The effect of applying the filter window is shown on the right side of Figure 4, where only the energy ring of A0 remains. The mode filtering process is important towards enhancing the ability for water ingress detection, and this is discussed further in the following next section.

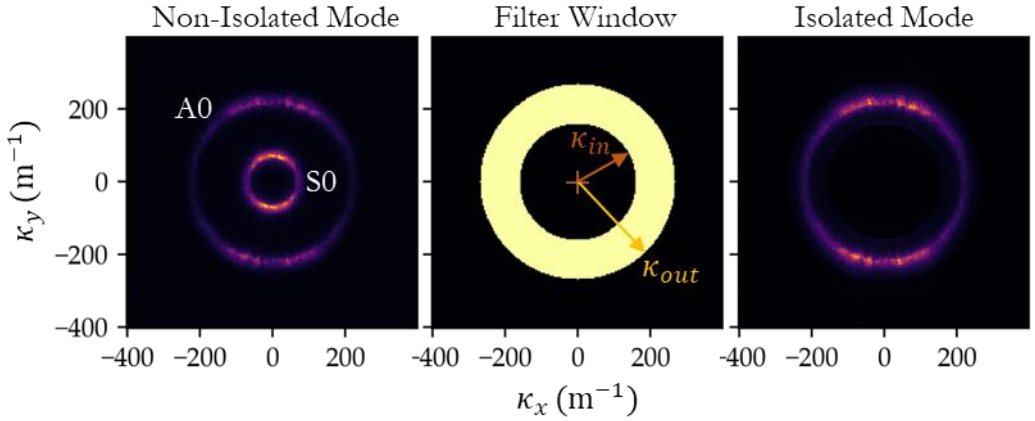

Figure 4: Mode filtering process. (a) Consolidated wavenumber-time domain data before filtering; (b) the filter window; and (c) the data after filtering.

For damage detection and visualization, the data for filtered and unfiltered modes are processed as images. Three visualization methods are used, including ultrasonic energy mapping (UEM), as reported in Ref. [17] but its wavenumber filter is replaced by the mode filter described in previous Equation 1, dominant frequency amplitude mapping (DFAM) [18], and spectral energy mapping (SEM). The UEM uses the simplified kinetic energy equation shown in Equation 2. On the other hand, the DFAM plots the highest amplitude from the frequency spectrum to show only the dominant amplitude generated to represent damage at a grid point as indicated in Equation 3. Lastly, SEM uses the amplitude from the broadband frequency and sum them all together to represent the grid position. The 3D spatio-temporal data needs to be transformed as 3D spatio-frequency data through one-dimensional FT along the time axis before being summed, which is presented in Equation 4.

$$\mathrm{UEM}(x,y) = \sum_{t=1}^{T} v(x,y,t)^2 \tag{2}$$

$$\mathrm{DFAM}(x,y) = V(x,y,f)_{max} \tag{3}$$

$$\mathrm{SEM}(x,y) = \sum_{f=1}^{F} V(x,y,f) \tag{4}$$

3. Results and Discussion

Through different methods of visualization, the results have been compared side by side in Figure 5 to help decide the best overall image visualization method suitable to detect the water ingress damage. There are three outputs for each visualization method, which are non-isolated mode, S0-isolated mode and A0-isolated mode, all of which pertain to the planar view of the specimen. It should be noted that this study focuses on the ability of mode isolation performance to visualize damage compared to a non-isolated mode based on these three outputs.

When using three different imaging methods through non-isolated mode, as represented in the left column in Figure 5, it is found that none of them is able to detect the water ingress, likely due to multiple modes causing interference that is obscuring the low-energy spots generated by the water ingress [19]. However, a wave-like pattern is observed in the images, possibly caused by the superposition of multiple

modes, which contributes to the increased noise level and further obscured the water ingress damage. To counter this, isolating a singular mode before image generation can prevent mode superposition and improve imaging capability. It is also observed that superposition could lead to inaccuracies in the signal and incorrect image representation, especially in non-isolated mode, which shows a wave-like pattern. However, this issue is not present in the images of the other cases with an isolated mode, leading to the conclusion that mode isolation can help to resolve the problem of signal inaccuracies caused by mode superposition and improve visual representation. Therefore, it is taken that selecting appropriate modes and preventing superposition can greatly improve the accuracy and effectiveness of image processing algorithms for detecting damage in materials.

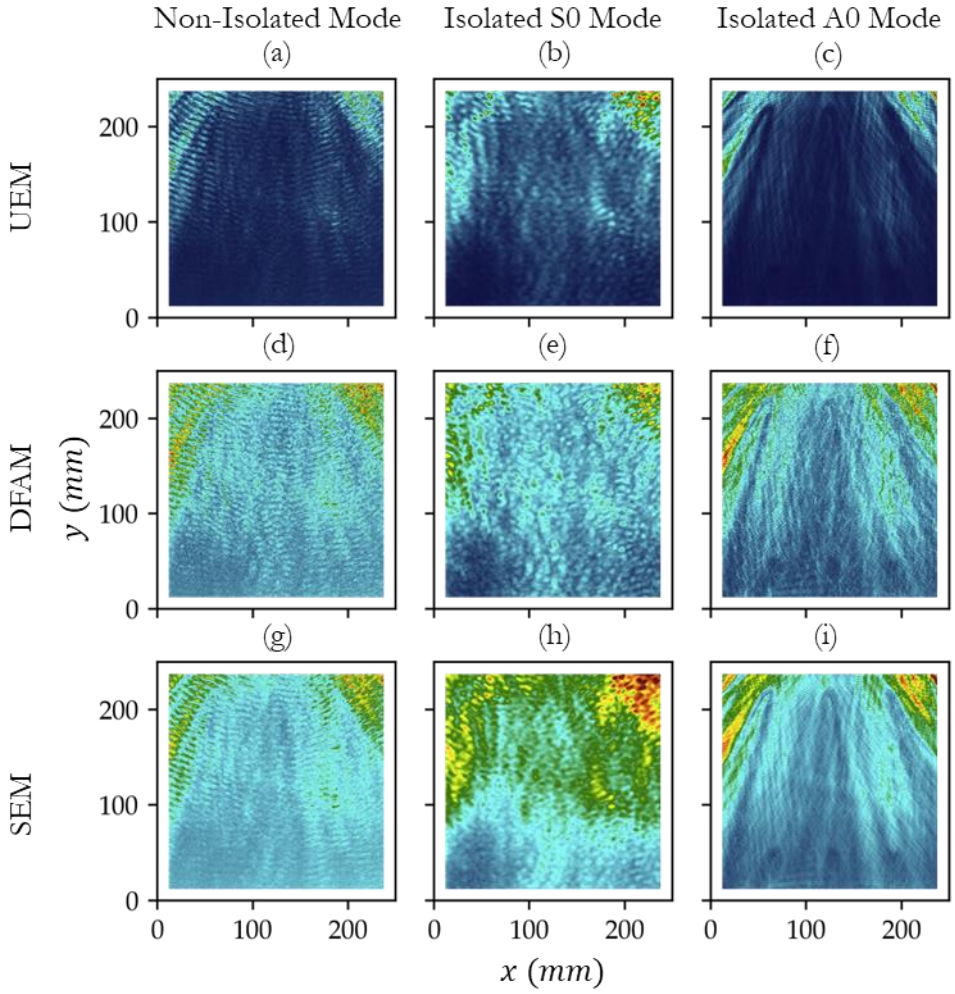

Figure 5: Comparison of damage in planar view using UEM (a to c), DFAM (d to f), and SEM (g to i). Unbalanced energy distribution was unavoidable due to directional wave propagation through honeycomb cells.

In the case of the isolated S0 mode, as represented in the middle column, none of the visualization methods has produced positive results as no information could be captured by this mode. This may be due to limitation of the S0 mode, which has a longer wavelength and penetrates through the specimen faster compared to the A0 mode, with less energy absorbed by the material. The depth of penetration of ultrasonic waves is determined by their frequency and wavenumber. However, since the S0 and A0 waves have the same frequency and the S0 wave travels at a faster velocity due to its longer wavelength, it experiences lower attenuation rates. This indicates that the S0 wave can travel further through the

material without losing its energy, resulting in less energy absorption in comparison to A0 wave, which has shorter wavelength and higher attenuation rate. Though the wavelength difference is not significant, the accumulation of small differences will eventually lead to significant change. In this case, it is desired to have a significant portion of the energy to be absorbed by the damage instead of being transferred away from it since that will reduce the chances of detecting the damage.

For the isolated A0 mode, as represented in the right column, all three methods appear to provide useful results but with different visualization capabilities. With UEM, water ingress is detectable at the top section close to the sensor while DFAM and SEM detect water ingress for the entire scanning area, particularly at the bottom section farther away from the sensor. These results vary as each method uses a different approach to visualize the damage. UEM employs the simplified kinetic energy equation to represent kinetic energy within the scan area, making it suitable for simple basic structures such as flat plates with uniform structural design and microstructures that have low damping properties. However, the high damping property of the aluminum honeycomb hinders the capability of UEM to visualize the whole area properly as the wave loses its energy too fast, resulting in a large dark area in the image seen in Figure 5(a) that represents a low-energy region. This indicates that a time-derived equation is not the best option. When visualizing complex structures such as honeycomb sandwiches, a frequency-derived equation is the more viable option due to its low susceptibility to material damping. This is because the frequency property of a wave remains constant regardless of the quick decrease of energy over time due to material damping, whereas time-derived equations are more susceptible to changes in material properties over time. Furthermore, using a frequency-derived equation provides detailed information about the structure by identifying different resonances and modes of vibration, which can help identify damage or defects that may not be easily visible using other methods.

To quantitatively compare the visualization methods, amplitude distribution along a horizontal line indicated in Figure 6(a), which crosses the position of amplitude drop caused by the water ingress, is extracted for analysis. To ensure meaningful comparison, the data for each visualization method have been normalized before extraction. Figure 6(b) to (c) show amplitude distributions for UEM, DFAM, and SEM, respectively, with yellow highlights representing regions with water-filled cells. Since the detection and visualization of water ingress require a magnitude contrast between the water-filled and unfilled cells, this contrast can serve as an evaluation metric to quantify the visibility of the water ingress. Equation 5 defines the contrast, where A represents the amplitude extracted from either the normalized UEM, DFAM, or SEM, it can be observed that $\mathbb{C} = 0.39 \times 10^2$, 1.86×10^2 and 2.79×10^2 (arbitrary unit, A.U.) for UEM, DFAM, and SEM, respectively. In other words, SEM exhibits 7.2 and 1.5 times higher contrast compared to UEM and DFAM, respectively. This simple analysis clearly indicates that SEM is the best visualization method among the three.

$$\mathbb{C} = \left|\min\left(A_{filled}\right) - \min\left(A_{unfilled}\right)\right| \tag{5}$$

Understanding material properties is crucial for accurate damage detection and visualization using image processing algorithms. Honeycomb structures with high damping properties pose a challenge for many visualization methods. Nevertheless, the use of a frequency-derived equation can provide more accurate and detailed information, which suits the application on complex structures with high damping properties. Although a direct explanation of this situation is not found in the literature, a few references have proven that using phase-based and frequency-based processing can improve the imaging quality compared to the amplitude-based counterpart [20]-[21]. By selecting appropriate visualization methods, the accuracy and effectiveness of the image processing algorithms can be improved. While both DFAM and SEM produce similar images based on the same frequency property, they may differ in sensitivity to different material properties or variations in the damage being detected. Therefore, it is important to carefully evaluate and select the suitable visualization methods based on specific material and type of

damage to be detected. Overall, the study highlights the importance of considering material properties and selecting suitable visualization methods when developing image-processing algorithms for detecting damage in materials. By doing so, the accuracy and effectiveness of these algorithms can be improved, and the algorithms can better detect and diagnose damage in a wide range of materials and structures.

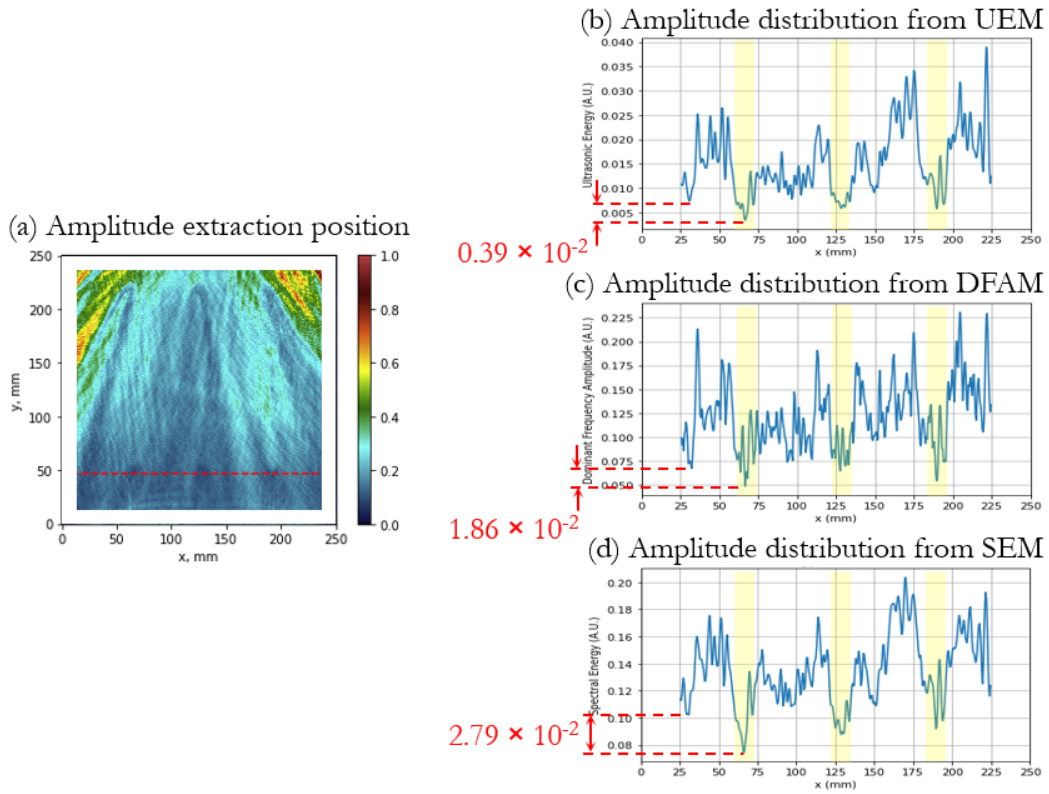

Figure 6: Definition of magnitude contrast $\mathbb{C}$. (a) Extraction of amplitude distribution along dashed red line. Getting $\mathbb{C}$ from the amplitude distribution for (b) UEM, (c) DFAM, and (d) SEM.

4. Conclusion

Water ingress in honeycomb cells of aerospace structures leads to many issues, including corrosion, disbonding, signal blockage and also increased weight, which can compromise the aircraft's safety and performance. Early detection of water ingress in non-destructive manner in honeycomb cells is complex and requires specific testing procedure, which is time-consuming and laborious. Therefore, this study is aimed to investigate the feasibility of using G-UPI to detect and visualize water ingress in honeycomb cells. The study has found that water ingress damage can be easily hidden even by a low level of noise and eliminating this noise could improve the imaging capability and increase the likelihood of detecting water ingress. Mode isolation is found to be an effective method to resolve the problem of noises that are caused by mode superposition and improve visual representation. The isolated S0 mode is found to be unsuitable for capturing any information regarding water ingress while the isolated A0 mode could yield useful results with varying degrees of visualization clarity. Three visualization methods: UEM, DFAM and SEM, are compared to determine the most suitable one for visualization of water ingress. It is found that a frequency-derived equation is a more viable option for visualizing complex structures such as honeycomb sandwich structures since it is less susceptible to material damping and can provide more accurate and detailed information about the structure being inspected. This is supported by the quantitative analysis based on magnitude contrast $\mathbb{C}$, which indicates that the frequency-based SEM is the best visualization method due to its 7.2 and 1.5 times higher contrast in comparison to UEM and

DFAM, respectively. In conclusion, G-UPI can be used for the detection of water ingress in honeycomb structures. Selecting appropriate result-processing methods based on the specific material being studied and the type of damage being detected is important for improving the accuracy and effectiveness of the visualization. Specifically, for the specimen used in this study, isolating the A0 mode and presenting the result as a SEM image is the best processing option. A few potential future works have been identified, which include the automation for determination of mode filter parameters κ_{in} and κ_{out} without human subjectivity, detection of partially-filled honeycomb cells and expansion of the method for water ingress detection in non-metallic honeycomb sandwich structures.

Acknowledgement

The authors acknowledge the support and funding for this research by Universiti Putra Malaysia through Industrial Research Grant Scheme of Tan Sri Syed Azman Syed Ibrahim's Endowment Fund (Account Vote No. 6338201-10801).

References

[1] H. A. Israr, T. S. Chwen, A. Abd Latif, K. J. Wong, S. S. R. Koloor, N. Yidris and M. Y. Yahya, 'Preliminary Structural Design of Coreless Spoiler by Topological Optimization', Processes, vol. 10, no. 10, 2076, 2022.

[2] G. Kim, R. Sterkenburg and W. Tsutsui, 'Investigating the Effects of Fluid Intrusion on Nomex® Honeycomb Sandwich Structures with Carbon Fiber Facesheets', Composite Structures, vol. 206, pp. 535–549, 2018.

[3] C. Ibarra-Castanedo, L. Brault, F. Marcotte, M. Genest, V. Farley and X. Maldague, 'Water Ingress Detection in Honeycomb Sandwich Panels by Passive Infrared Thermography using a High-Resolution Thermal Imaging Camera', Proceedings of SPIE, vol. 8354, pp. 20-27, 2012.

[4] X. Xu, W. Huo, F. Li and H. Zhou, 'Classification of Liquid Ingress in GFRP Honeycomb Based on One-Dimension Sequential Model Using THz-TDS', Sensors, vol. 23, no. 3, 3, 2023.

[5] V. Vavilov, A. Klimov, D. Nesteruk and V. Shiryaev, 'Detecting Water in Aviation Honeycomb Structures by Using Transient Infrared Thermographic NDT', Proceedings of AEROSENSE 2003, Orlando, USA, April 2003.

[6] C. C. Chia, J. R. Lee, J. S. Park, C. Y. Yun and J. H. Kim, 'New Design and Algorithm for an Ultrasonic Propagation Imaging System', Proceedings of Defektoskopie 2008, Brno, Czech Republic, November 2008.

[7] C. C. Chia, S. G. Jang, J. R. Lee and D. J. Yoon, 'Structural Damage Identification Based on Laser Ultrasonic Propagation Imaging Technology', Proceedings of SPIE, vol. 7389, 73891S 2009.

[8] C. C. Chia, S. Y. Lee, M. Y. Harmin, Y. Choi and J. R. Lee, 'Guided Ultrasonic Waves Propagation Imaging: A Review', Measurement Science and Technology, vol. 34, no. 5, 052001, 2023.

[9] Z. Tian, W. Xiao, Z. Ma and L. Yu, 'Dispersion Curve Regression–Assisted Wideband Local Wavenumber Analysis for Characterizing Three-Dimensional (3D) Profile of Hidden Corrosion Damage', Mechanical Systems and Signal Processing, vol. 150, 107347, 2021.

[10] P. Kudela, M. Radzieński and W. Ostachowicz, 'Identification of Cracks in Thin-Walled Structures by Means of Wavenumber Filtering', Mechanical Systems and Signal Processing, vol. 50–51, pp. 456-466, 2015.

[11] D. Girolamo, H. Y. Chang and F. G. Yuan, 'Impact Damage Visualization in a Honeycomb Composite Panel Through Laser Inspection using Zero-Lag Cross-Correlation Imaging Condition', Ultrasonics, vol. 87, pp. 152-165, 2018.

[12] F. Gao, J. Hua, L. Wang, L. Zeng and J. Lin, 'Local Wavenumber Method for Delamination Characterization in Composites with Sparse Representation of Lamb Waves', IEEE Transactions on Ultrasonics, Ferroelectrics and Frequency Control, vol. 68, no. 4, pp. 1305-1313, 2021.

[13] J. Monchalin, 'Laser-Ultrasonics: From the Laboratory to Industry', AIP Conference Proceedings, vol. 700, no. 1, pp. 3-31, 2004.

[14] H. Lamb, 'On Waves in an Elastic Plate', Proceedings of the Royal Society of London. Series A, Containing Papers of a Mathematical and Physical Character, vol. 93, no. 648, 648, 1917.

[15] J. L. Rose, Ultrasonic Guided Waves in Solid Media, Cambridge University Press, 2014.

[16] E. B. Flynn, S. Y. Chong, G. J. Jarmer and J. R. Lee, 'Structural Imaging through Local Wavenumber Estimation of Guided Waves', NDT & E International, vol. 59, pp. 1-10, 2013.

[17] S. H. Abbas, T. C. Truong and J. R. Lee, 'FPGA-based Ultrasonic Energy Mapping with Source Removal Method for Damage Visualization in Composite Structures', Advanced Composite Materials, vol. 26, 2017.

[18] M. A. Shahrim, M. Y. Harmin, F. I. Romli, C. C. Chia and J. R. Lee, 'Damage Visualization based on Frequency Shift of Single-Mode Ultrasound-Guided Wavefield', Journal of Aeronautics, Astronautics and Aviation, vol. 54, no. 3, pp. 297-305, 2022.

[19] F. Ling, H. Chen, Y. Lang, Z. Yang, K. Xu and D. Ta, 'Lamb Wave Tomography for Defect Localization using Wideband Dispersion Reversal Method', Measurement, vol. 216, 112965, 2023.

[20] N. Wadhwa, M. Rubinstein, F. Durand and W. T. Freeman, 'Phase-based Video Motion Processing', ACM Trans. Graph., vol. 32, no. 4, pp. 1-10, 2013.

[21] P. Fromme, F. Bernhard and B. Masserey, 'High-Frequency Guided Ultrasonic Waves to Monitor Corrosion Thickness Loss', AIP Conference Proceedings, vol. 1806, no. 1, 1, 2017.